## Anisotropic band structure of TiS<sub>3</sub> nanoribbon revealed by polarized photocurrent spectroscopy

Cite as: Appl. Phys. Lett. 117, 073101 (2020); https://doi.org/10.1063/5.0019828 Submitted: 25 June 2020 . Accepted: 29 July 2020 . Published Online: 18 August 2020

Zhen Lian, Zeyu Jiang, Tianmeng Wang 🗓, Mark Blei, Ying Qin, Morris Washington, Toh-Ming Lu, Sefaattin Tongay, Shengbai Zhang, and Su-Fei Shi 📵







### ARTICLES YOU MAY BE INTERESTED IN

Atomistic defects as single-photon emitters in atomically thin MoS<sub>2</sub> Applied Physics Letters 117, 070501 (2020); https://doi.org/10.1063/5.0018557

Enhancing the photoelectrical performance of graphene/4H-SiC/graphene detector by tuning a Schottky barrier by bias

Applied Physics Letters 117, 071102 (2020); https://doi.org/10.1063/5.0012566

Ultrahigh photovoltage responsivity of PEDOT:PSS-silicon hybrid heterojunction photodiodes Applied Physics Letters 117, 073301 (2020); https://doi.org/10.1063/5.0007685









# Anisotropic band structure of TiS<sub>3</sub> nanoribbon revealed by polarized photocurrent spectroscopy

Cite as: Appl. Phys. Lett. **117**, 073101 (2020); doi: 10.1063/5.0019828 Submitted: 25 June 2020 · Accepted: 29 July 2020 · Published Online: 18 August 2020







Zhen Lian, Zeyu Jiang, Tianmeng Wang, Dark Blei, Ying Qin, Morris Washington, Toh-Ming Lu, Sefaattin Tongay, Shengbai Zhang, and Su-Fei Shi, 4, 10

#### **AFFILIATIONS**

- Department of Chemical and Biological Engineering, Rensselaer Polytechnic Institute, Troy, New York 12180, USA
- <sup>2</sup>Department of Physics, Rensselaer Polytechnic Institute, Troy, New York 12180, USA
- School for Engineering of Matter, Transport and Energy, Arizona State University, Tempe, Arizona 85287, USA

#### **ABSTRACT**

A re-discovered member of the layered material family, Titanium Trisulfide (TiS<sub>3</sub>), has attracted intense research interest recently for the possibility of realizing an exciton insulator in the monolayer limit. However, due to their quasi-one-dimensional nature, thin TiS<sub>3</sub> flakes are typically in the form of nanoribbons that are challenging to characterize by optical absorption spectra, due to their small cross section. Here, we employ a sensitive photocurrent spectroscopy technique to probe the absorption of a thin TiS<sub>3</sub> nanoribbon in a field-effect transistor configuration. We have found a significant modification of the band structure of the thin TiS<sub>3</sub> nanoribbon, compared to its bulk counterpart. In addition, the polarization-dependent photocurrent spectra of thin TiS<sub>3</sub> nanoribbons exhibit greatly enhanced anisotropy compared to that of a thick TiS<sub>3</sub> device. The atomically thin TiS<sub>3</sub> flake, thus, not only provides an exciting platform for investigating many-body physics but also enables anisotropic quantum optoelectronics.

Published under license by AIP Publishing. https://doi.org/10.1063/5.0019828

Among the growing family of vast two-dimensional (2D) materials, there exists a class of layered materials with a quasione-dimensional (1D) structure that has attracted intense research interest recently, which includes ZrS<sub>3</sub>, ZrSe<sub>3</sub>, HfTe<sub>3</sub>, TiS<sub>3</sub>, etc. 1-5 The 2D materials in this family naturally possess large electrical and optical anisotropy and often exhibit exotic quantum physics when thinned down to atomic thicknesses. 1-11 For example, TiS3 was recently predicted to be a promising candidate for hosting the long-searched exciton insulator at the monolayer limit. 12 However, limited by the quasi-1D nature, the thin flakes of such layered materials are typically in the form of nanoribbons, with the width comparable to or even much smaller than the diffraction limit of the light. As a result, optical spectroscopy, which has been a powerful tool to study the band structure of 2D materials through reflectance/absorption measurements, 13 cannot probe the thin flake of such quasi-1D layered materials easily due to the small cross section that limits the amount of detectable optical signals. Meanwhile, photocurrent spectroscopy can reveal the absorption information by measuring the photocurrent response as a function of the excitation photon energy, 14,15 thus providing

a sensitive probe of the band structure, especially for the semiconducting device with a low dark current. Although the anisotropic photocurrent response has been demonstrated in  $\mathrm{TiS}_3$  flake-based photodetectors, <sup>8</sup> no absorption spectrum has been reported for quasi-1D thin flakes of  $\mathrm{TiS}_3$  yet, to the best of our knowledge.

In this work, by fabricating both thick ( $\sim$ 200 nm thick) and thin ( $\sim$ 15 nm thick) TiS<sub>3</sub> flakes into field-effect transistor (FET) devices, we reveal the band structure of both the thin and thick TiS<sub>3</sub> flakes through photocurrent spectroscopy. Our study shows that the thick TiS<sub>3</sub> flake possesses a bandgap around 0.90 eV and is promising for infrared optoelectronics. In contrast, the band structure of thin TiS<sub>3</sub> is modified by the quantum confinement, and the bandgap is increased to about 0.96 eV. Also, the absorption resonance is significantly modified as well. While the thick sample shows two major absorption resonances at 1.23 eV and 1.41 eV, the thin sample exhibits a single peak at 1.34 eV. Our work demonstrates that photocurrent spectroscopy is a powerful tool to probe the band structure and excitonic physics in quasi-1D layered materials, and TiS<sub>3</sub> nanoribbon is a promising candidate for anisotropic optoelectronics in the near-infrared regime.

Department of Electrical, Computer and Systems Engineering, Rensselaer Polytechnic Institute, Troy, New York 12180, USA

a) Author to whom correspondence should be addressed: shis2@rpi.edu

TiS<sub>3</sub> crystals were synthesized via the chemical vapor transport method. One-gram stoichiometric mixture of elemental titanium and sulfur was loaded in a quartz ampule [1.5 cm outer diameter (OD) and 20 cm in length] and sealed under evacuation at 10<sup>-5</sup>Torr. Crystal growth was allowed for 7 days in a two-zone furnace with precursors in the hot zone (550 °C) and crystallization in the cold zone (450 °C). We mechanically exfoliate TiS<sub>3</sub> flakes on the 285 nm SiO<sub>2</sub>/Si substrate. 7,16 Raman spectra of the flakes are in good agreement with previous reports<sup>5,17,18</sup> (see the supplementary material for details). We further fabricate TiS3 into two-terminal FET devices, with the schematic shown in Fig. 1(a). Metal contacts are defined by shadow masks or standard E-beam lithography process followed by E-beam evaporation of 3 nm/20 nm Ti/Au. Figures 1(b) and 1(c) show the typical optical microscope image of the device made of thick and thin TiS3 flakes, with thicknesses of  $\sim$ 200 nm and  $\sim$ 15 nm, respectively. It is worth noting that thin TiS<sub>3</sub> is barely visible under the optical microscope, as the width is only  $\sim$ 100 nm. The length of the nanoribbon, however, and is as long as  $\sim 10 \,\mu \text{m}$  [Fig. 1(c)].

We then measure the photocurrent spectra of the two different devices, recording the photocurrent response as a function of the excitation photon energy. For such measurements, we use a supercontinuum white laser source (Fianium or YSL Photonics) combined with a monochromator (with a grating of groove density 600 g/mm) and optical filters (550 nm longpass filter for visible spectra and 850 nm longpass filter for infrared spectra) to generate monochromatic excitation light (bandwidth  $\sim$ 1.0 nm). The sample is mounted in an optical cryostat, cooled with liquid nitrogen. A polarizer and a  $\lambda$ / 2 Fresnel rhomb are used to convert the excitation laser into polarized light with the polarization aligned along either the a or b direction of the nanoribbon [directions perpendicular or parallel to the 1D chain, shown in Figs. 1(d) and 1(e)], which can be determined under the confocal optical microscope. The excitation laser is then focused with an objective to a relatively large spot (typically  $10-40 \mu m$ ) that uniformly illuminates the whole conducting channel of the sample, and a low excitation intensity (0.2-1 mW/cm<sup>2</sup>) is used to ensure a linear response from the sample (see the supplementary material for details). The laser excitation is modulated with a mechanical chopper operating

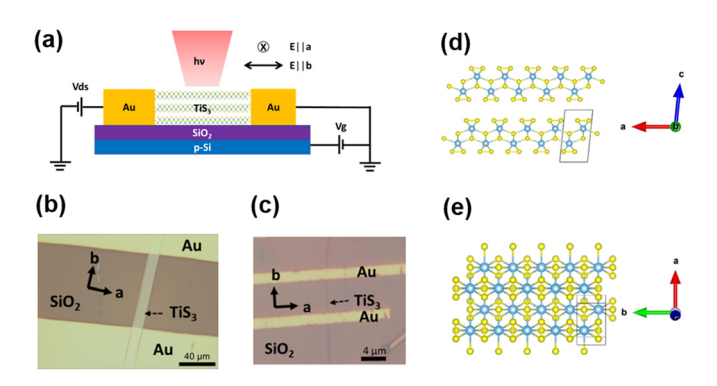


**FIG. 1.** Two-terminal TiS $_3$  FET devices on the SiO $_2$ /Si substrate. (a) The schematic of the two-terminal TiS $_3$  FET device and the configuration of polarization-dependent photocurrent spectroscopy. (b) and (c) show optical microscope images of the two devices based on the thick (b) and thin (c) TiS $_3$  flakes. (d) and (e) display the out-of-plane and in-plane atomic structures of the TiS $_3$  crystal produced using VESTA. Yellow spheres: S atoms. Blue spheres: Ti atoms.

at 636 Hz. A DC bias of 1 V is applied to the TiS<sub>3</sub> device, and the resulting photocurrent signal is collected with a current amplifier and a lock-in amplifier. After we measure the photocurrent spectra of the TiS<sub>3</sub> device, the sample is immediately replaced with a commercially available Si or InGaAs detector to measure the power spectrum of the laser spot, which is then used to normalize the photocurrent response as  $I_{pc}(h\nu)$ . The ultra-high sensitivity of this setup is evident from the photocurrent spectra shown in Figs. 2(a) and 2(b), with the signal to noise ratio as high as more than three orders of magnitude.

The normalized photocurrent response from the two different devices exhibits distinctively different behaviors, as shown in Figs. 2(a) and 2(c). First, for the optical field aligned along the b axis, there are two pronounced peaks for the thick flake device [Fig. 2(a)] located at  $\sim$ 1.23 eV and  $\sim$ 1.41 eV (the dip at  $\sim$ 1.17 eV is an artifact due to the laser spectrum, see the supplementary material for details). In contrast, the photocurrent spectrum of the thin flake device [Fig. 2(b)] with the optical field aligned along the b axis only shows one peak at  $\sim$ 1.34 eV. Second, the photocurrent spectra for the polarization along the b axis and the a axis can be used to define the anisotropy as  $A = \frac{I_{PC}(b) - I_{PC}(a)}{I_{L-}(I_k) + I_{L-}(A)}$ . For the thick flake device [Fig. 2(a)], Anisotropy A can be as large as 0.71 and 0.43 at the resonance at  $\sim$ 1.23 eV and  $\sim$ 1.41 eV, respectively. However, this anisotropy quickly diminishes as the excitation photon energy increases, approaching zero at the excitation photon energy of 1.8 eV. In contrast, the anisotropy of the thin flake device [Fig. 3(c)] not only exhibits enhanced anisotropy (0.86) at the resonance excitation of ~1.34 eV but also retains the anisotropy for high excitation photon energy,  $\sim$ 0.46, for the excitation photon energy of 1.8 eV.

As the photocurrent is proportional to the absorption, <sup>15,19</sup> we speculate that the distinct photocurrent spectra of the thick and thin TiS<sub>3</sub> devices originate from the quantum confinement-modified band structure. We first investigate the rising of the photocurrent spectra, as shown in Figs. 2(b) and 2(d). In the linear absorption regime, the normalized photocurrent  $I_{pc}(h\nu)$  is linked to the absorption coefficient  $\alpha(h\nu)$  by the expression:<sup>15</sup>

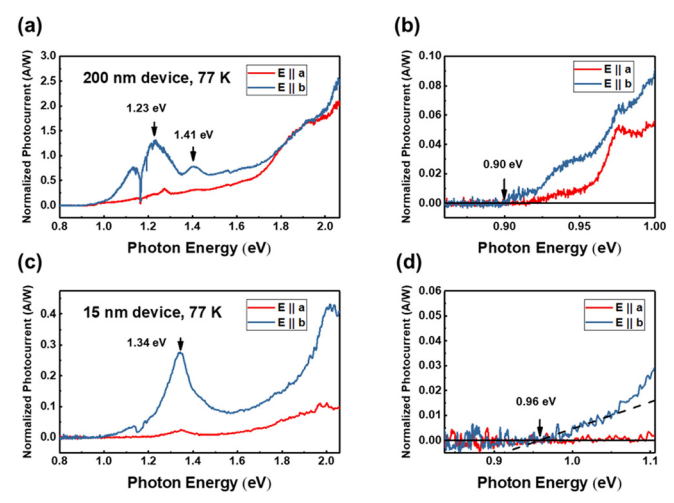


**FIG. 2.** Photocurrent spectra of  $TiS_3$  FET devices. (a) and (c) show polarized photocurrent spectra of the thick and thin  $TiS_3$  flake devices measured at 77 K. (b) and (d) show corresponding zoom-in spectra near the absorption cutoffs.

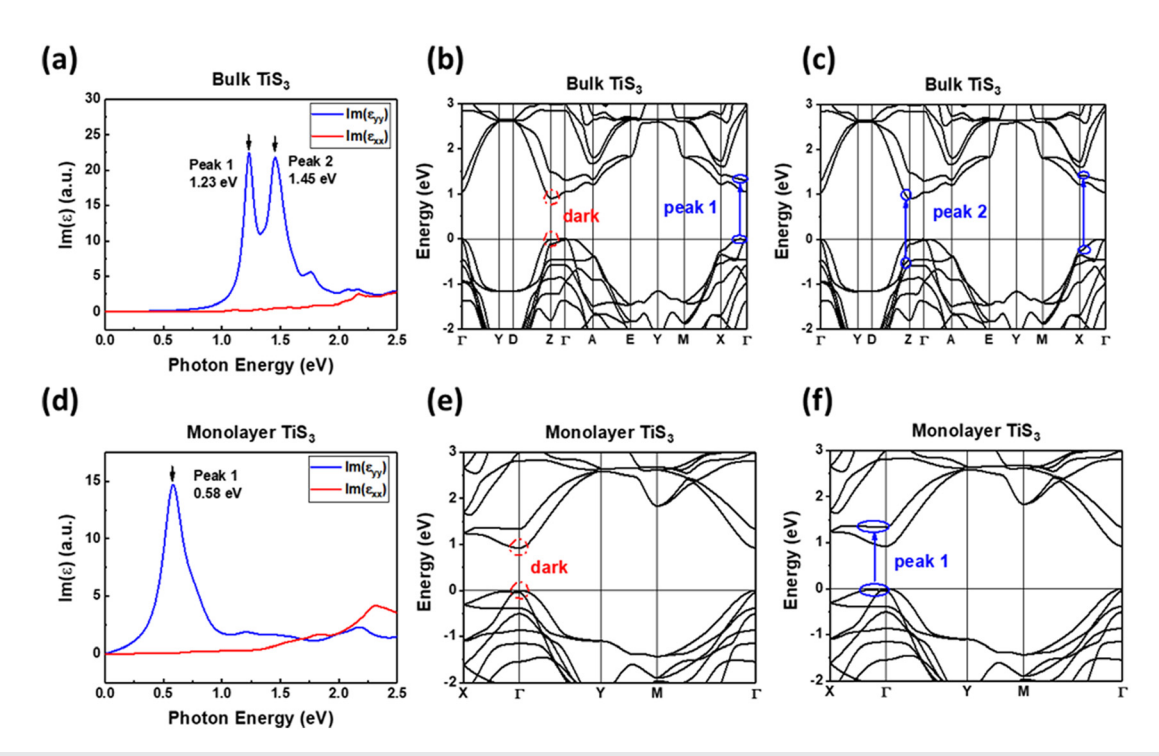


**FIG. 3.** Calculated band structure and imaginary part of the dielectric constant of bulk and monolayer  $TiS_3$ . (a) and (d) show imaginary part of the dielectric constant along b and a directions in (a) bulk and (d) monolayer  $TiS_3$ . (b) and (c) show the same calculation of the bulk  $TiS_3$  band structure with the different transitions labeled, corresponding to the peaks in (a). (e) and (f) show the same calculation of monolayer  $TiS_3$ , labeled with the dark ground state and the peak 1 transition in (d). High symmetry points:  $\Gamma$  (0, 0, 0), Y (0, 0.5, 0), D (0, 0.5, 0.5), Z (0, 0, 0.5), A (0.5, 0, 0.5), E(0.5, 0.5, 0.5), M (0.5, 0.5), D (0.5, 0.5), D (0.5, 0.5), C (0.5, 0.5),

$$I_{pc}(h\nu) = \frac{\eta e}{h\nu} \alpha(h\nu),$$

where e is the electron charge,  $h\nu$  is the photon energy, and  $\eta$  is the photogain and is independent of  $h\nu$ . The corresponding bandgap  $E_g$  can be determined by reading the photon energy corresponding to the photocurrent cutoff since the value of kT is significantly smaller than the bandgap of TiS<sub>3</sub>. Figure 2(b) shows that, for the thick TiS<sub>3</sub>, the bandgap  $E_g = 0.90 \, \text{eV}$ . This result is consistent with the value  $(0.97-1.10 \, \text{eV})^{20-25}$  reported previously for the bulk TiS<sub>3</sub>. For the thin TiS<sub>3</sub> device, Fig. 2(d) shows a bandgap of  $0.96 \, \text{eV}$ , which indicates a modification of the bandgap owing to quantum confinement.

We further perform first-principles calculations to understand the different normalized photocurrent spectra shown in Figs. 2(a) and 2(c). The calculated band structure for the bulk and monolayer TiS<sub>3</sub> is shown in Figs. 3(b), 3(c) and 3(e), 3(f), respectively [Figs. 3(b) and 3(c) show the same calculation results with different transitions labeled, the same for Figs. 3(e) and 3(f)]. As shown in Fig. 3(b), bulk TiS<sub>3</sub> possesses an indirect bandgap, and its conduction band minimum (CBM) and valence band maximum (VBM) are located at Z and  $\Gamma$  points, respec-The calcutively, consistent with the previous theoretical study.<sup>26</sup> lated value of the bandgap is corrected by the experimental value of 0.90 eV with a scissor operator. The imaginary part of dielectric constant  $Im(\varepsilon)$ , which is proportional to the absorption, is further calculated as a function of excitation photon energy by solving the Bethe-Salpeter equation (BSE) [Fig. 3(a)]. We denote the dielectric function along the b axis and a axis by  $\varepsilon_{yy}$  and  $\varepsilon_{xx}$  respectively. It is evident from Fig. 3(a) that  $Im(\varepsilon_{vv})$  shows two pronounced peaks at 1.23 eV and 1.45 eV, which are in excellent agreement with our experimental values of 1.23 eV and 1.41 eV. In contrast, these peaks do not appear in the spectrum of  $Im(\varepsilon_{xx})$ , also consistent with our experimental observation [Fig. 2(a)]. The optical transitions corresponding to each peak are labeled with arrows in Figs. 3(b) and 3(c). The lowest direct transition at the Z point [marked as the red dashed circle in Fig. 3(b)] is forbidden for the in-plane polarizations due to the inversion symmetry of the wave function near the band edge, similar to the case of  $\Gamma$  excitons in the monolayer<sup>11</sup> [shown in Fig. 3(e)]. The first peak at 1.23 eV in Fig. 2(a) is a result of the transition shown in Fig. 3(b), with the energy difference between the corresponding conduction band and valence band being  $\sim$ 1.30 eV. As a result, the exciton binding energy is  $\sim$ 70 meV for the observed peak of 1.23 eV in Fig. 2(a). The second peak at 1.41 eV in Fig. 2(a) has two major contributions, which, as shown in Fig. 3(c), originate from the bands near X and Z points and correspond to the calculated 1.45 eV peak in Fig. 3(a). These transitions correspond to the energy difference around 1.51 eV, indicating an exciton binding energy around 60 meV.

We also perform first-principles calculations for the  $TiS_3$  monolayer. The obtained band structure and dielectric function are consistent with the results of previous theoretical studies. <sup>11,27</sup> As shown in Fig. 3(e), due to the absence of the Z point in the 2D Brillouin zone, monolayer  $TiS_3$  possesses a direct bandgap of 0.92 eV at the  $\Gamma$  point. It is worth noting that the energies of the bands near the  $\Gamma$  point only show minor changes compared to the bulk  $TiS_3$ . This unusual thickness dependence behavior is due to the orbital components of the CBM and the VBM, which originate from the center atoms in the unit

cell and are not sensitive to interlayer interaction. Therefore, there is a transition [peak 1 in Fig. 3(f)] similar to that associated with peak 1 in bulk TiS3. However, the band structure near the X point is drastically different, and the Z point disappears with the out-of-plane dispersion of the band structure. As a result, the transition corresponding to peak 2 in bulk TiS3 cannot find its counterpart in the monolayer limit. These results are clearly shown in the spectrum of  $Im(\epsilon_{yy})$ , which is significantly different from that of bulk TiS3 and has only one resonance peak at 0.58 eV, which is a result of the exciton originating from the valence band near -0.03 eV along the  $\Gamma-X$  direction to the conduction band at around 1.35 eV.  $^{11}$ 

Our experimental data of the thin TiS3 device are more like the monolayer TiS<sub>3</sub>, and we further analyze the theoretical calculations to compare with our data quantitatively. First, we believe that our observed peak at 1.34 eV corresponds to the optical transition shown as peak 1 in Fig. 3(e). First, according to our previous discussion, the energies of the bands involved in this transition are not a sensitive function of the thickness. Second, the resonance at 0.58 eV shown in Fig. 3(d) is a result of large exciton binding energy of ~800 meV for monolayer TiS3. Considering that the thickness of 15 nm is likely much larger than the exciton radius, we expect a similar exciton binding energy in the thin TiS<sub>3</sub> flake compared to the thick TiS<sub>3</sub> ( $\sim$ 200 nm which is 70 meV. As a result, the exciton absorption resonance for 15 nm TiS<sub>3</sub> is expected at  $\sim$ 1.31 eV. Finally, we have to consider the experimentally extracted bandgap for the thin TiS<sub>3</sub> flake, 0.96 eV, which is slightly larger than the calculated bandgap of 0.92 eV for monolayer TiS<sub>3</sub> that is obtained by adopting the same shift to the bandgap correction as the bulk TiS<sub>3</sub>. Therefore, the expected exciton resonance for the thin TiS<sub>3</sub> flake should be at 1.35 eV. This expectation is in excellent agreement with our observed resonance at 1.34 eV [Fig. 2(c)].

Finally, we discuss the different anisotropy observed in thick and thin TiS<sub>3</sub> flakes experimentally. The theoretical calculations show similar anisotropy behaviors for bulk and monolayer TiS3: large anisotropy in absorption at resonance and negligible anisotropy at high excitation photon energy. Our photocurrent spectra of the thick TiS<sub>3</sub> device are consistent with this picture. In contrast to the experimental observation in the thick TiS<sub>3</sub> device, the thin TiS<sub>3</sub> device retains a reasonably large anisotropy in the photocurrent response at high excitation photon energy, besides a large anisotropy at resonance excitation. This is because the thin TiS<sub>3</sub> flake is in the form of nanoribbons, which has a width of ~100 nm, smaller than the wavelength. As a result, the geometry anisotropy contributes to the absorption process and results in the additional photocurrent anisotropy observed experimentally. The thick TiS<sub>3</sub> flake has a width of  $\sim$ 11  $\mu$ m and does not have a contribution from geometry anisotropy. We note here that, due to the monoclinic structure of TiS3, the off diagonal components of the imaginary dielectric tensor might not be zero and might affect the experimentally measured anisotropy. However, our calculations show that such contributions are not significant in our measurements (see the supplementary material).

In summary, by exploiting polarization-dependent photocurrent spectroscopy, we have measured the absorption spectra of the quasi-1D thin flake of TiS<sub>3</sub>, which is hard to obtain using other convention optical spectroscopy methods. The photocurrent spectra of thin TiS<sub>3</sub> are significantly different from those of the thick TiS<sub>3</sub> flake (bulk). Our results are in excellent agreement with the first-principles calculations,

showing that the TiS<sub>3</sub> thin flake possesses a band structure that is close to the monolayer TiS<sub>3</sub> flake, but significantly different from the bulk TiS<sub>3</sub>. Therefore, the thin TiS<sub>3</sub> flake provides a platform to investigate intriguing quantum physics in the quantum confined TiS<sub>3</sub>. In addition, the greatly enhanced anisotropy of the quasi-1D thin flake of TiS<sub>3</sub> promises future applications of polarized optoelectronics.

See the supplementary material for Raman and AFM characterization of TiS<sub>3</sub> flakes, power dependence of the photocurrent spectra, calculated off diagonal components of the imaginary dielectric tensor, and the method of density functional theory (DFT) calculations.

We thank Zhipeng Li and Shengnan Miao for helpful discussions. We also thank Stephanie Westaway and Brayton Pierce for their help with sample preparation. This work was supported by the NY State Empire State Development's Division of Science, Technology and Innovation (NYSTAR) through Focus Center-NY-RPI Contract No. C150117. This work made use of the Micro- and Nano-Fabrication Clean Room Facility and the Nanoscale Characterization Core at Rensselaer Polytechnic Institute. T.W. and S.-F.S. acknowledge support from ACS PRF through Grant No. 59957-DNI10. S.T. acknowledges support from Nos. DOE-SC0020653, NSF DMR 1552220, DMR 1904716, and NSF CMMI 1933214. Z.J. and S. Zhang were supported by the U.S. DOE Grant No. DE-SC0002623. The supercomputer time sponsored by the National Energy Research Scientific Center (NERSC) under DOE Contract No. DE-AC02-05CH11231 and the Center for Computational Innovations (CCI) at RPI are also acknowledged. S.-F.S and S. Zhang acknowledge the support from a KIP Grant from RPI. S.-F.S. also acknowledges support from AFOSR through Grant No. FA9550-18-1-0312 and NSF Career Award No. DMR-1945420.

#### **DATA AVAILABILITY**

The data that support the findings of this study are available from the corresponding author upon reasonable request.

### **REFERENCES**

- <sup>1</sup>Y. Jin, X. Li, and J. Yang, Phys. Chem. Chem. Phys. **17**(28), 18665 (2015).
- <sup>2</sup>A. Pant, E. Torun, B. Chen, S. Bhat, X. Fan, K. Wu, D. P. Wright, F. M. Peeters, E. Soignard, H. Sahin, and S. Tongay, Nanoscale 8(36), 16259 (2016).
- <sup>3</sup>D. Pacilé, M. Papagno, M. Lavagnini, H. Berger, L. Degiorgi, and M. Grioni, Phys. Rev. B **76**(15), 155406 (2007).
- <sup>4</sup>J. Li, J. Peng, S. Zhang, and G. Chen, Phys. Rev. B 96(17), 174510 (2017).
- <sup>5</sup>J. O. Island, R. Biele, M. Barawi, J. M. Clamagirand, J. R. Ares, C. Sánchez, H. S. J. Van Der Zant, I. J. Ferrer, R. D'Agosta, and A. Castellanos-Gomez, Sci. Rep. 6, 1–7 (2016).
- <sup>6</sup>A. Khatibi, R. H. Godiksen, S. B. Basuvalingam, D. Pellegrino, A. A. Bol, B. Shokri, and A. G. Curto, 2D Mater. 7(1), 015022 (2019).
- <sup>7</sup>J. O. Island, M. Barawi, R. Biele, A. Almazán, J. M. Clamagirand, J. R. Ares, C. Sánchez, H. S. J. Van Der Zant, J. V. Álvarez, R. D'Agosta, I. J. Ferrer, and A. Castellanos-Gomez, Adv. Mater. 27(16), 2595 (2015).
- <sup>8</sup>S. Liu, W. Xiao, M. Zhong, L. Pan, X. Wang, H. X. Deng, J. Liu, J. Li, and Z. Wei, Nanotechnology **29**(18), 184002 (2018).
- <sup>9</sup>N. Papadopoulos, R. Frisenda, R. Biele, E. Flores, J. R. Ares, C. Sánchez, H. S. J. Van Der Zant, I. J. Ferrer, R. D'Agosta, and A. Castellanos-Gomez, Nanoscale 10(26), 12424 (2018).
- <sup>10</sup>M. Van Der Donck and F. M. Peeters, Phys. Rev. B **98**(23), 235401 (2018).
- <sup>11</sup>E. Torun, H. Sahin, A. Chaves, L. Wirtz, and F. M. Peeters, Phys. Rev. B **98**(7), 075419 (2018)
- <sup>12</sup>Z. Jiang, Y. Li, S. Zhang, and W. Duan, Phys. Rev. B **98**(8), 081408 (2018).

- <sup>13</sup> A. Chernikov, T. C. Berkelbach, H. M. Hill, A. Rigosi, Y. Li, O. B. Aslan, D. R. Reichman, M. S. Hybertsen, and T. F. Heinz, Phys. Rev. Lett. 113(7), 076802 (2014).
- <sup>14</sup>J. Trägårdh, A. I. Persson, J. B. Wagner, D. Hessman, and L. Samuelson, J. Appl. Phys. **101**(12), 123701 (2007).
- <sup>15</sup>A. R. Klots, A. K. M. Newaz, B. Wang, D. Prasai, H. Krzyzanowska, J. Lin, D. Caudel, N. J. Ghimire, J. Yan, B. L. Ivanov, K. A. Velizhanin, A. Burger, D. G. Mandrus, N. H. Tolk, S. T. Pantelides, and K. I. Bolotin, Sci. Rep. 4, 6608 (2014).
- <sup>16</sup>K. S. Novoselov, A. K. Geim, S. V. Morozov, D. Jiang, Y. Zhang, S. V. Dubonos, I. V. Grigorieva, and A. A. Firsov, Science 306(5696), 666 (2004).
- <sup>17</sup>K. Wu, E. Torun, H. Sahin, B. Chen, X. Fan, A. Pant, D. P. Wright, T. Aoki, F. M. Peeters, E. Soignard, and S. Tongay, Nat. Commun. 7(1), 12952 (2016).
- <sup>18</sup>A. Lipatov, M. J. Loes, H. Lu, J. Dai, P. Patoka, N. S. Vorobeva, D. S. Muratov, G. Ulrich, B. Kästner, A. Hoehl, G. Ulm, X. C. Zeng, E. Rühl, A. Gruverman, P. A. Dowben, and A. Sinitskii, ACS Nano 12(12), 12713 (2018).
- <sup>19</sup>M. Buscema, J. O. Island, D. J. Groenendijk, S. I. Blanter, G. A. Steele, H. S. J. Van Der Zant, and A. Castellanos-Gomez, Chem. Soc. Rev. 44(11), 3691 (2015).
- <sup>20</sup>I. J. Ferrer, J. R. Ares, J. M. Clamagirand, M. Barawi, and C. Sánchez, Thin Solid Films 535(1), 398 (2013).
- <sup>21</sup>A. J. Molina-Mendoza, M. Barawi, R. Biele, E. Flores, J. R. Ares, C. Sánchez, G. Rubio-Bollinger, N. Agraït, R. D'Agosta, I. J. Ferrer, and A. Castellanos-Gomez, Adv. Electron. Mater. 1(9), 1500126 (2015).

- <sup>22</sup>Y. Niu, R. Frisenda, E. Flores, J. R. Ares, W. Jiao, D. Perez de Lara, C. Sánchez, R. Wang, I. J. Ferrer, and A. Castellanos-Gomez, Adv. Opt. Mater. 6(19), 1800351 (2018).
- <sup>23</sup>I. J. Ferrer, M. D. Maciá, V. Carcelén, J. R. Ares, and C. Sánchez, Energy Procedia 22(1), 48 (2012).
- <sup>24</sup>C. G. Hawkins and L. Whittaker-Brooks, ACS Appl. Nano Mater. 1(2), 851 (2018).
- <sup>25</sup>M. Barawi, E. Flores, I. J. Ferrer, J. R. Ares, and C. Sánchez, J. Mater. Chem. A 3(15), 7959 (2015).
- <sup>26</sup>J. Dai and X. C. Zeng, Angew. Chem., Int. Ed. **54**(26), 7572 (2015).
- <sup>27</sup>J. Kang and L. W. Wang, Phys. Chem. Chem. Phys. **18**(22), 14805 (2016).
- <sup>28</sup>G. Zhang, A. Chaves, S. Huang, F. Wang, Q. Xing, T. Low, and H. Yan, Sci. Adv. 4(3), eaap9977 (2018).
- <sup>29</sup>L. Li, J. Kim, C. Jin, G. J. Ye, D. Y. Qiu, F. H. Da Jornada, Z. Shi, L. Chen, Z. Zhang, F. Yang, K. Watanabe, T. Taniguchi, W. Ren, S. G. Louie, X. H. Chen, Y. Zhang, and F. Wang, Nat. Nanotechnol. 12(1), 21 (2017).
- 30 D. Y. Qiu, F. H. Da Jornada, and S. G. Louie, Nano Lett. 17(8), 4706 (2017).
- <sup>31</sup>H. P. Komsa and A. V. Krasheninnikov, Phys. Rev. B **86**(24), 241201 (2012).
- 32Y. Yu, Y. Yu, Y. Cai, W. Li, A. Gurarslan, H. Peelaers, D. E. Aspnes, C. G. Van De Walle, N. V. Nguyen, Y. W. Zhang, and L. Cao, Sci. Rep. 5, 16996 (2015).
- <sup>53</sup>G. W. Mudd, S. A. Svatek, T. Ren, A. Patanè, O. Makarovsky, L. Eaves, P. H. Beton, Z. D. Kovalyuk, G. V. Lashkarev, Z. R. Kudrynskyi, and A. I. Dmitriev, Adv. Mater. 25(40), 5714 (2013).
- 34K. Momma and F. Izumi, J. Appl. Crystallogr. 44(6), 1272 (2011).